Non-Standard Electroconvection in a Bent Core Nematic

D. Wiant and J. T. Gleeson
Department of Physics, Kent State University, Kent, OH 44242 USA

N. Éber and K. Fodor-Csorba
Research Institute for Solid State Physics and Optics, Hungarian Academy of Sciences,
H-1525 Budapest, P.O.B.49, Hungary

A. Jákli and T. Tóth-Katona
Liquid Crystal Institute, Kent State University, Kent, OH 44242 USA

We characterize three non-standard electrohydrodynamic instabilities in nematic liquid crystals composed of bent core molecules. In addition to their shape, another important attribute of this material is that the anisotropy in the electrical conductivity changes sign as the frequency of the applied electric field changes. These instabilities do not appear to fit within the standard model for electroconvection. The first instability creates a pattern with stripes parallel to the initial director orientation, with a wavelength about equal to the separation of the cell plates. The next is the previously reported prewavy instability. The third instability is optically and dynamically identical to the prewavy instability, but is distinguished by different threshold behavior.

I. Introduction

Nematic liquid crystals (NLC), when driven out of equilibrium, can exhibit a rich variety of electroconvection (EC) patterns. These patterns result from the strong coupling between the NLC's orientational degrees of freedom, described by a unit vector field $\hat{n}$ (the director), the flow field, and the induced electric field. Because the anisotropies in the electrical transport properties (dielectric constant and conductivities) play such a critical role in EC, it is convenient to categorize NLC's according to the signs of these quantities. Specifically, the dielectric anisotropy, ϵ_a is $\epsilon_\parallel - \epsilon_\perp$, where $\epsilon_\parallel$ is the dielectric permittivity for an electric field parallel to the director and $\epsilon_\perp$ is the component measured perpendicular to the director. Similarly the conductivity anisotropy, σ_a, describes the difference between the parallel and perpendicular components of the conductivity. There are four combinations of these anisotropies that can occur in a NLC, which can be written in the compact notation $(++)$, $(+-)$, $(-+)$, and $(--)$. Here the first sign represents the sign of the dielectric anisotropy and the second that of the conductivity anisotropy. For electro-optic information display purposes $(++)$ materials are by far the most commonly employed, while the vast majority of EC experimental and theoretical work has focussed on $(-+)$ materials. The Carr-Helfrich theory [1–4] predicts that EC will occur both in this latter case as well as in the unusual $(+-)$ situation.

For a system with an initial planar alignment, we choose a coordinate system such that the z-axis runs perpendicular to the plates confining the liquid crystal, the x-axis is parallel to the initial director orientation, and the y-axis is perpendicular to the other two axes. (This coordinate system will be used in the remainder of this paper.) The Carr-Helfrich theory predicts, for the planar $(-+)$ case, spontaneous formation of a pattern of convective rolls perpendicular (or in some cases at an angle) to the x-axis with a periodicity close to twice the spacing between the plates, d. This occurs as the applied potential difference is raised above a threshold voltage, V_{th}. This is the scenario at low frequencies, and is called the conductive regime. The theory also predicts that above a certain cut-off frequency, f_c, there exists a pattern of shorter wavelength stripes ($\lambda < d$), which also run perpendicular to the x-axis. This is the dielectric regime. These patterns are formed due to a periodic modulation of the director in the xz-plane, which can be explained by charge transport and convection effects. Both of these regimes have been extensively studied over the past few decades (see [5] and references therein).

http://www.e-lc.org/docs/2005_04_15_13_57_18

Recently studies of the other situations $(+-)$ [6], $(++)$ [7], and $(--)$ [8–10] also have started to attract attention. Recent work on $(--)$ and $(++)$ NLCs in a planar orientation has shown EC not described by the Carr-Helfrich theory. Of particular interest to this paper is the $(--)$ situation. Here patterns of oblique rolls with wavelengths of the order of d, running roughly parallel to the x-axis, have been observed [8,9]. The mechanism which drives this pattern formation is not yet understood. Additionally, certain NLCs exhibit the so called prewavy instability. The prewavy (or wide domain) instabilities have been experimentally observed and theoretically discussed by several authors [11–21]. The prewavy pattern consists of a set of alternating dark and bright stripes, which are most easily viewed between crossed polarizers. The stripes run in the y-direction, perpendicular to the initial director direction. The prewavy instability corresponds to a periodic modulation of the director in the xy-plane, unlike that described by the Carr-Helfrich theory which predicts director modulation in the xz-plane. The prewavy pattern can further be distinguished from the Carr-Helfrich type behavior by its long wavelength, $\lambda \sim 4d$–$8d$. The forementioned characteristics of the prewavy instability have been clearly defined, but little is understood of the mechanism that produces this instability. The prewavy instability shares some common features with somewhat better understood models, such as the anisotropic inertia mode and the isotropic electrolyte mode, but ultimately differs from both these instabilities [18]. The prewavy instability is believed to be caused by an isotropic pattern formation mechanism, but further examination of this instability is needed to verify this conjecture.

Liquid crystals composed of bent core, or banana shaped, molecules have been the subject of a great deal of research in recent years due to their formation of ferroelectric phases [22–24], as well as the possibility of biaxial nematic phases [25–28]. The ways in which the bent molecules arrange and interact amongst themselves suggest a wealth of new phases [29] not seen in traditional LC's composed of rod-shaped molecules. Although many questions have been answered about banana shaped LCs, there still is much that is not yet understood about these materials. As they become more prevalent in science and industry it is important to have a thorough understanding of banana shaped LCs and their behavior under different conditions.

Few bent core molecules exhibit a nematic phase [30–34], and up to now very little work has been done on EC in bent core nematics (BCN). This paper will examine EC in the BCN labeled ClPbis10BB [35]. This compound shows three distinct frequency regions of EC instabilities, none of which seem to be explained by the Carr-Helfrich theory or a weakly nonlinear analysis, along with a region where no EC occurs.

In the remainder of this paper we will first discuss our experimental setup and methods. Then we will present and discuss the physical parameters of ClPbis10BB that are relevant for EC. Next, we will discuss each of the instabilities in order of their appearence with increasing frequency, beginning with the parallel stripe pattern observed at very low frequencies. This is followed by a wide stripe pattern, similar to the prewavy pattern, that is present between $30 - 1000Hz$. Then there is a region that does not show any EC up to about $5000Hz$. This is followed by another wide stripe pattern. We will examine the thresholds and characteristics of each region and attempt to begin to explain their formation mechanisms.

II. Experimental

The experiments were performed on the bent core nematic liquid crystal 4-chloro-1,3-phenylene bis4-[4'-(9-decenyloxy)benzoyloxy]benzoate (ClPbis10BB) [35]. Its schematic chemical structure is shown in Fig. 1. ClPbis10BB exhibits a monotropic nematic phase upon cooling from 78 ± 1°C to about 60°C. This compound, with no added impurities was placed in commercially obtained sandwich type cells [36] with d of 10μm to 50μm. The surfaces of the cells were coated with transparent electrodes (indium tin oxide). The area of the conducting regions ranged from 100mm^2 on the 10μm cell to 50mm^2 on the 50μm cell. Cells for all EC and splay Freedericksz transition measurements were treated for planar alignment. All optical measurements were made using either a Zeiss Axiovert or a Nikon Optiphot polarizing microscope and a Panasonic CCD camera with a frame grabber. For these measurements the temperature was stabilized to ±0.1°C using an Instec HS-1 hotstage. An *ac* voltage was sustained across the plates of the cell, which subjected the liquid crystal to an applied electric field $\vec{E} = (\sqrt{2}V/d)cos(2\pi ft)\hat{z}$.

III. Results and Discussion

1. *Material Properties*

Because little is known about either a new material such as ClPbis10BB in particular, or BCNs in general, we have measured some of the physical parameters important for EC. Specifically, the dielectric constants

http://www.e-lc.org/docs/2005_04_15_13_57_18

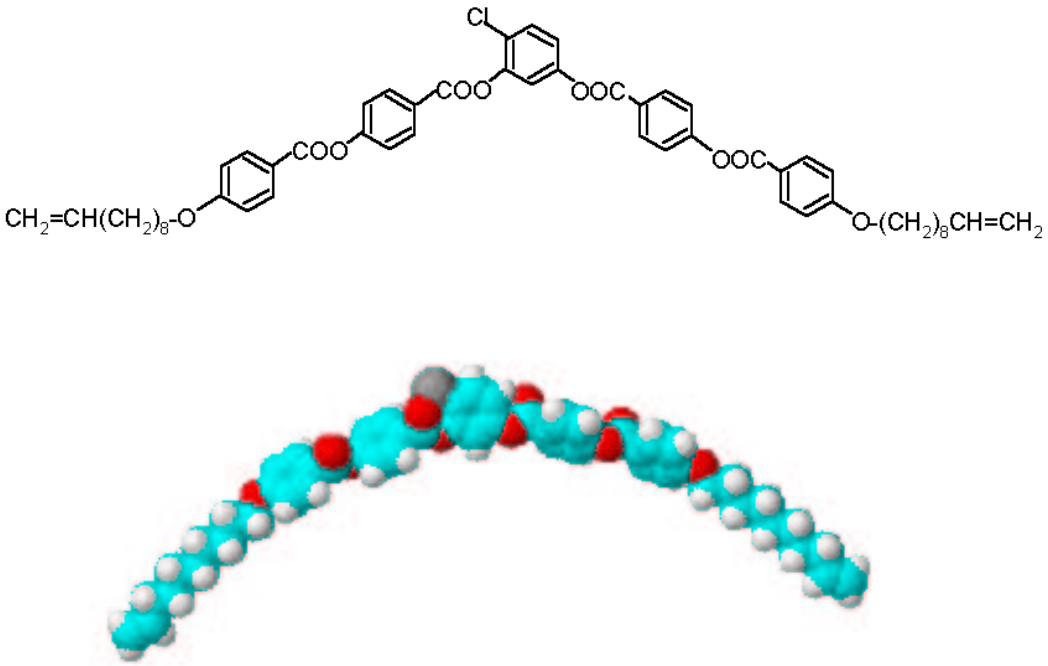

Figure 1: Schematic chemical structure and space filling model of 4-chloro-1,3-phenylene bis4-[4'-(9-decenyloxy)benzoyloxy]benzoate.

and conductivities, the splay and bend elastic constants, the anisotropy of the diamagnetic susceptibility (χ_a) and the rotational viscosity (γ_1) have been determined.

Two sets of measurements of electrical transport properties were made by monitoring the capacitance, C, and conductance, g, of planar-aligned samples as they underwent the magnetic field induced Freedericksz transition [4]. The first, at a single probe frequency of 1kHz, employed an auto-balancing Andeen Hagerling capacitance bridge to measure the capacitance and loss of a relatively thick sample ($d = 55.1\mu$m) as a function of magnetic field H. At this thickness we were able to reach approximately 6-7 times the Freedericksz threshold field, H_F. At $H = 0$ the perpendicular components, $\epsilon_\perp$ and $\sigma_\perp$, could be measured directly. From data at $H >> H_F$ we could accurately extrapolate to infinite field, and thus obtain the parallel components, $\epsilon_\parallel$ and $\sigma_\parallel$. An example of such data is shown in Fig. 2. The value of H_F gives us the ratio K_{11}/χ_a, while the slope of the $C(H)$ curve just above onset yields the ratio K_{33}/K_{11} [37].

The second measurement used a Quadtech 1920 frequency scanning LCR meter. For this measurement we used a thinner sample ($d = 25\mu$m), with which we could raise the magnetic field above H_F but could not accurately extrapolate data to infinite field. Therefore, these measurements; made at 70°C, 75°C, and 77°C; only yielded the signs of ϵ_a and σ_a, but as functions of frequency. For the entire available frequency range (1Hz $-$ 100kHz) at all three temperatures, with the magnetic field on ($H > H_F$) the capacitance was smaller than with the field off. Thus, $\epsilon_\perp > \epsilon_\parallel$, i.e. $\epsilon_a < 0$ for all temperatures and frequencies employed.

Conductance measurements revealed that σ_a has some unique features not usually seen in rod-like nematics. High precision measurements on the $d = 55.1\mu$m sample at 1kHz show the relative conductivity anisotropy, $\sigma_a/\sigma_\perp$, to be less than 0.03 in magnitude and to become negative at about 3 degrees below the clearing point, T_{NI}. However, as the frequency is changed at a constant temperature the conductivity anisotropy changes sign twice, the sign being positive in an intermediate band between about 1.5kHz and 8kHz for the $d = 25\mu$m sample. Figure 3 demonstrates this behaviour at 70°C. The frequencies where the sign inversion of σ_a occur depend on the temperature. The lower sign inversion frequency falls into the range 1500 $-$ 1900Hz, the upper sign inversion occurs between 8100 $-$ 11000Hz. Upon increasing the temperature both sign inversion frequencies shift toward higher f. This is also exhibited in Fig. 8.

The double sign inversion of σ_a can be attributed to a dielectric relaxation process occurring in the

http://www.e-lc.org/docs/2005_04_15_13_57_18

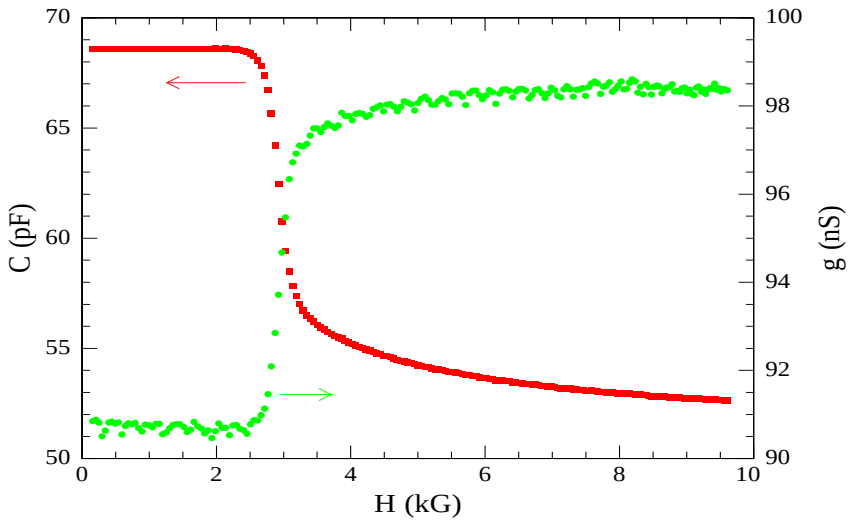

Figure 2: Example of the variation of the measured capacitance and conductance with magnetic field.

specified frequency range. The dielectric loss has a frequency dependent contribution to the conductivity, which has a maximum at the relaxation frequency f_r and decays when moving to either higher or lower f. The loss due to the relaxation in the parallel component can raise $\sigma_{\|}$ enough to induce the change from $\sigma_a < 0$ to $\sigma_a > 0$ and back near f_r. The relaxation in the parallel component should be accompanied by a reduction of $\epsilon_{\|}$. Indeed, the capacitance of the the cell with the magnetic field on showed a decrease as frequencies were increased, while no significant frequency dependence was found in the field off case (i.e. for $\epsilon_{\perp}$ and $\sigma_{\perp}$). Dielectric relaxation frequencies of nematics are generally in the MHz range (see [38] and referneces therein). An f_r at about 4kHz (as shown in Fig. 3) is quite unusual. The rare cases in which nematics are known to exhibit relaxation in the kHz range are, however, characterized by a (single) sign inversion of ϵ_a, and they show no change in the sign of σ_a, i.e. they exhibit a different behavior than the BCN tested.

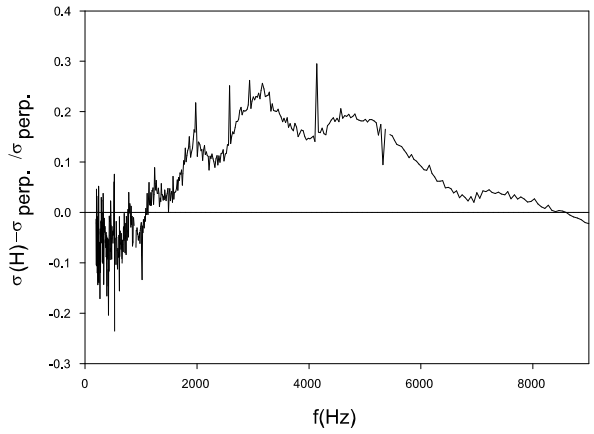

Figure 3: This figure shows $\frac{\sigma(H)-\sigma_{\perp}}{\sigma_{\perp}}$, where $\sigma(H)$ is the (nearly) parallel component measured in the Freedericksz state with $H = 10.9$kG. σ_a is negative from 1Hz to roughly 1500Hz, positive for 1500 $\rightarrow$ 8100Hz, and then negative again up to the end of the measurement at 100kHz. These measurements were made on the 25μm sample at 70°C.

By monitoring the rate of change of the capacitance as the magnetic field is raised above the critical field in a planar cell, we obtained the orientational relaxation time $\tau_1 = \gamma_1 d^2/K_{11}\pi^2$, which yielded γ_1. We note that although backflow is expected in this geometry, its presence should not effect the time constant [39]. Finally, we measured the critical potential difference for the electric field induced bend Freedericksz transition

by monitoring the light transmitted through a homeotropically aligned sample ($d = 50\mu$m) placed between crossed polarizers. This gives the ratio K_{33}/ϵ_a. Neither K_{11} nor K_{33} vary greatly with temperature and both are between 1.5 and 2.5pN, with K_{33} larger than K_{11}. Thus, ClPbis10BB appears to possess similar elastic properties to rod-like calamitic liquid crystals (see [4] and references therein). Likewise, $\chi_a \approx 2 \times 10^{-7}$ (in SI units) is comparable to that of calamitics (see [4] and references therein). Interestingly however, γ_1 was found to range between 1.8 and 2.5 Pa·s, which is more than thirty times larger than that of typical rod-like nematics such as methoxy benzylidene butylaniline (MBBA) [40] or pentylcyanobiphenyl (5CB) [41,42]. This clearly is a major contributor to the extreme slowness with which the various patterns respond to changes in the driving voltage and/or frequency.

2. Electroconvection

ClPbis10BB exhibits 4 very different scenarios at threshold as the frequency is changed. These 4 regimes are defined using Fig. 4, which shows threshold voltages, V_{th}, for the sample at 75°C. All V_{th} values referred to were found by slowly raising the voltage then waiting 15 minutes at the final voltage to see if a pattern became visible through crossed, or nearly crossed, polarizers. This process was then repeated with the voltage being lowered. The first region at $1 - 28$Hz, which we call the parallel stripes (PS) regime, has a linear frequency dependence of the threshold voltage as shown in the insetof Fig. 4. The next region is the prewavy2 (PW2) regime, from $28 - 1000$Hz. It is followed by the empty region (ER) at $1000 - 5000$Hz, and finally by the prewavy1 (PW1) regime above 5000Hz.

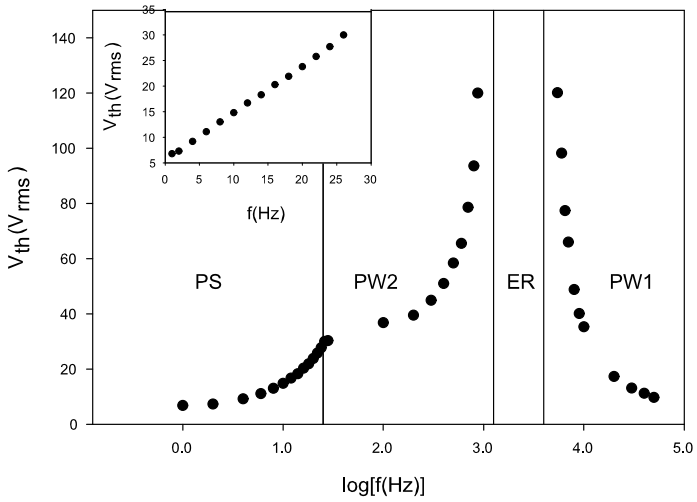

Figure 4: Threshold curve for a 15μm sample at 75°C in the v-$log(f)$ plane. Below 28Hz parallel stripes (PS) are observed. From $28 - 1000$Hz a wide stripe pattern (PW2) is seen. The region from $1000 - 5000$Hz does not show any EC (ER). Above 5000Hz another wide stripe pattern (PW1) is observed. Regions are separated by solid lines. Inset shows PS threshold versus frequency to better demonstrate the linearity of the threshold curve in this region.

ClPbis10BB is $(--)$ in the PS region. The patterns observed here (Fig. 5a) are similar to those seen by Kochowska, et al. [8] in $(--)$ calamitic liquid crystals. The PS pattern consists of stripes with wavelengths slightly less than d, which went from parallel to slightly oblique with regard to the initial director orientation. The best contrast was achieved when the polarizer and analyzer were a few degrees from perpendicular. This suggests that the director had periodic modulations in the xy-plane. At 75°C the pattern was visible from $1 - 24$Hz. Then at $25 - 27$Hz a coexistence of the parallel stripes and the perpendicular wide stripes (PW2, to be described below) could be seen (Fig. 5b). At frequencies above 28Hz, PS was no longer present. When the voltage was increased well above the threshold in PS a turbulent state could be observed (Fig. 5d).

V_{th} for PS is shown versus frequency at three different temperatures in Fig. 6(a). The frequency dependence of V_{th} remains linear while the temperature is changed. The slope of the threshold curve decreases as

http://www.e-lc.org/docs/2005_04_15_13_57_18

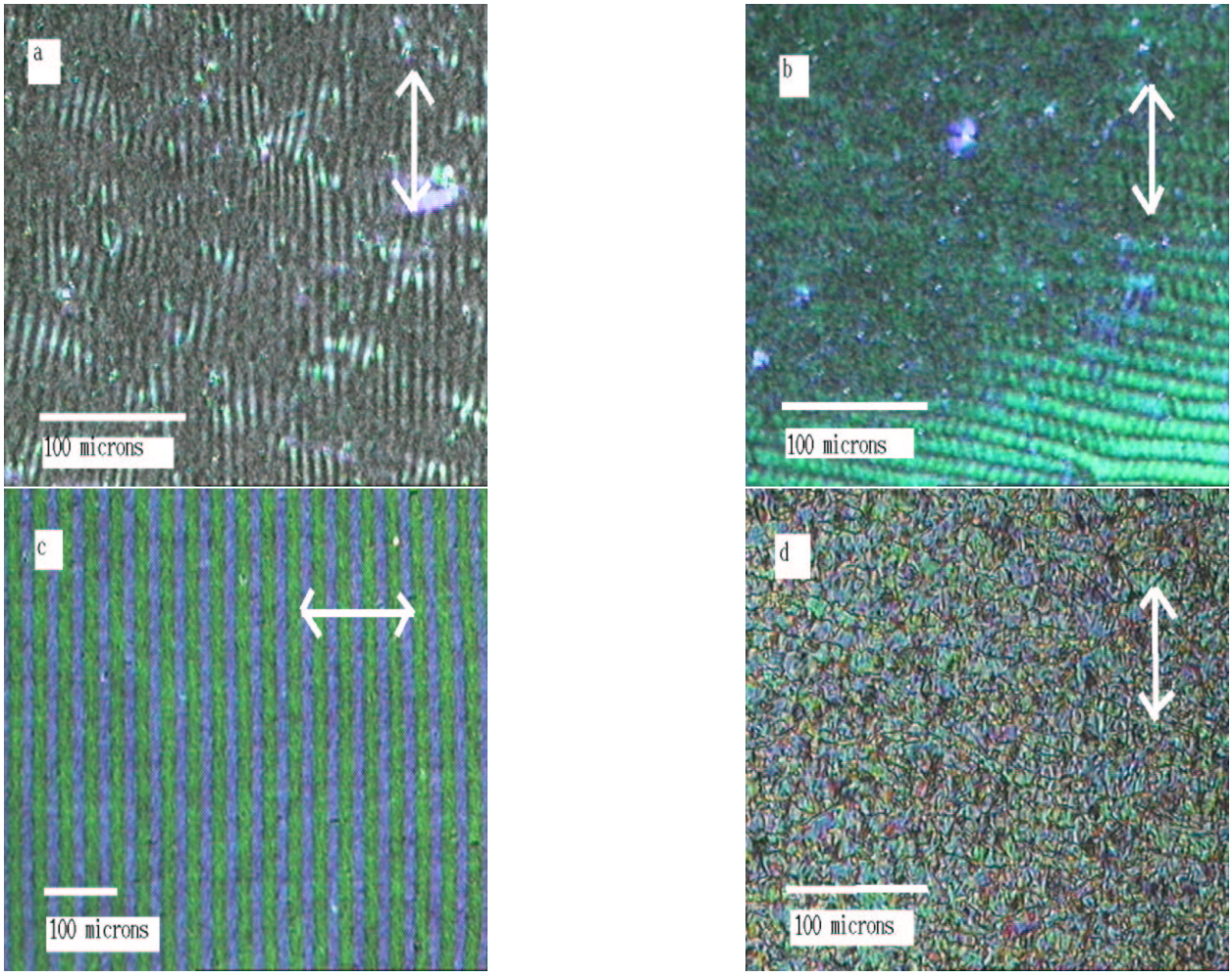

Figure 5: (a) PS at 12Hz and 28V$_{rms}$. (b) PS and PW2 coexisting at 26Hz and 32V$_{rms}$. (c) PW2 at 200Hz and 25V$_{rms}$. (d) Turbulent state at 6Hz and 28V$_{rms}$, which is well above threshold at this frequency. Images (a) and (b) were taken with a 15μm sample at 75°C, (c) and (d) with a 10μm sample at 70°C. White arrow indicates rubbing direction of cell plates and length scale represents 100μm in each picture.

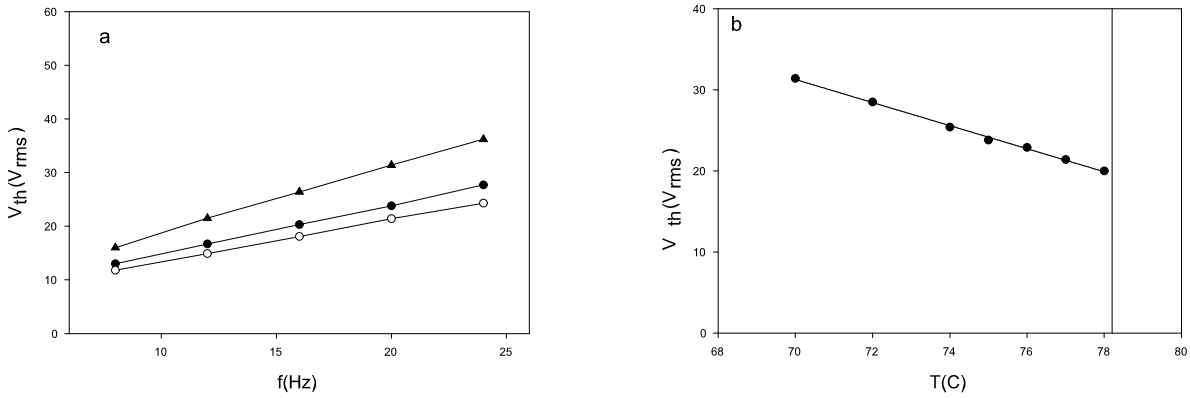

Figure 6: (a) V_{th} versus frequency in the PS regime. Solid triangles, solid circles, and open circles represent data at 70°C, 75°C, and 77°C, respectively. (b) Temperature dependence of V_{th} at 20Hz in the PS regime. The clearing point is at 78.2°C. Both measurements were made on a 15μm sample.

http://www.e-lc.org/docs/2005_04_15_13_57_18

the temperature is increased. Figure 6(b) shows that V_{th} decreases monotonically as the clearing point is approached, which suggests that an isotropic mode might be responsible for the formation of this pattern. In contrast, the threshold voltage of an anisotropic mode, that is a mechanism dependent on the inherent anisotropy of the dielectric and conductive properties of the substance, is generally expected to show a divergence as the temperature comes closer to the clearing point. This occurs because the voltage needed to drive the instability is inversely proportional to the anisotropy of the system (ϵ_a and σ_a), which becomes very small as T goes to T_{NI}.

Flow patterns were not observed in the PS region. This is probably due to difficulties in detecting and measuring flow. The parallel stripes were narrow and tend to form in small, localized regions, which make it difficult to follow the flow of a dust particle.

Next we will discuss the ER. This region is unique because it appears to be void of any EC. The potential difference was increased up to 130V_{rms}, which in this case produced an electric field of about 12.3V/μm. This voltage was nearly large enough to cause dielectric breakdown, yet no EC was observed in this frequency range. Figure 7 shows the reciprocals of $V_{th}(f)$ in both the regions neighbouring the ER (PW1 at higher and PW2 at lower frequencies) for a sample at 75°C. Each set of points could be well fitted with a straight line. Assuming that the linearity of $1/V_{th}(f)$ survives even at higher voltages, the lines were extrapolated to zero. The intersections enclose a band of frequency which suggests that the increase of the V_{th} on both sides of ER is not simply due to a divergence at a single frequency. Rather it points to an absence of EC at all voltages. Figure 8 shows that the PW1 region extends towards lower frequencies as the temperature is increased, i.e. the width of ER is reduced, but even within 0.5° of the clearing point the inverse of $V_{th}(f)$ still indicated an ER of finite width.

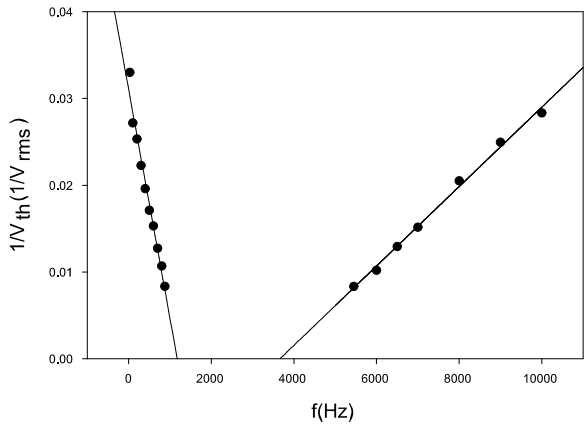

Figure 7: The linear fits (solid lines) to $1/V_{th}(f)$ for PW2 (at low f) and PW1 (at high f) at 75°C indicate that an ER exists even as $V_{th}(f)\rightarrow\infty$.

PW1 and PW2 are domains with wide stripes that run perpendicular to the x-axis. The two modes are so named because PW1 shows nearly identical characteristics to the prewavy mode described earlier [17,18], and PW2 shows many similarities to PW1. PW1 and PW2 are visually indistinguishable under a polarizing microscope, but are clearly separated in frequency by the ER and exhibit different threshold behaviors.

PW1 and PW2 show nearly identical optical and dynamic properties. The two patterns do seem to differ in a few regards though, which will be discussed before their similarities. First the shape of the $V_{th}(f)$ curve seems to show a stronger frequency dependence for PW2 then it does for PW1. Figure 8 shows that $V_{th}(f)$ for PW2 has only a slight temperature dependence, while $V_{th}(f)$ for PW1 seems to show a marked shift to lower f as the temperature is increased. Next, $V_{th}(T)$ for PW1 monotonically decreases as the clearing point is approached, while $V_{th}(T)$ for PW2 increases in the vicinity of T_{NI}, as shown in Fig. 9. (In some samples V_{th} for PW2 has been found to diverge at the clearing point. The deviations between samples are believed to be related to the individual sample conductivities.)

http://www.e-lc.org/docs/2005_04_15_13_57_18

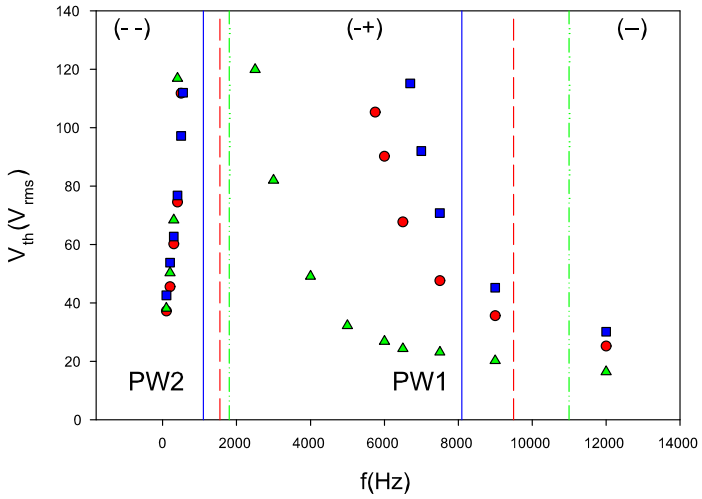

Figure 8: Frequency dependence of the threshold voltages for PW1 and PW2. Squares, circles and triangles represent V_{th} at 70°C, 75°C, and 77°C, respectively. The solid, dashed, and dashed-dotted lines mark the frequencies where the sign of of σ_a changes at 70°C, 75°C, and 77°C, respectively. These measurements were made on a 25μm cell. V_{th}(T) for PW1 shows a strong temperature dependence, while V_{th}(T) for PW2 shows only a slight temperature dependence.

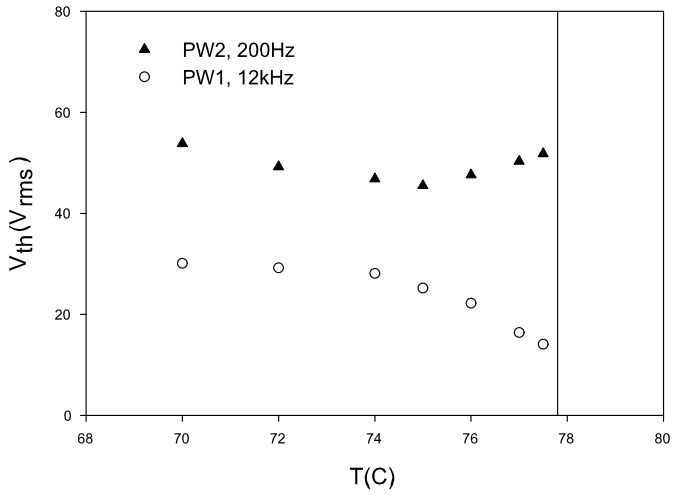

Figure 9: Temperature dependence of threshold voltages for the prewavy regimes. Solid triangles represent $V_{th}(T)$ for PW2 at 200Hz, open circles represent $V_{th}(T)$ for PW1 at 12000Hz. The clearing point is at 77.8°C. Both measurements were made on a 25μm sample.

Figure 8 shows that a change in the sign of the conductivity anisotropy occurs near the point where $V_{th}(f)$ for PW2 appears to diverge. The location of the higher sign inversion frequency of σ_a seems to show a stronger temperature dependence than that of the lower frequency one, moreover, $V_{th}(f)$ for PW1 appears not to be affected by the higher frequency sign inversion. These observations taken together seem to suggest that PW2 is driven by an anisotropic mechanism, while PW1 is driven by an isotropic one. However, although an increase in V_{th} for PW2 is always seen near the clearing point, a divergence is not always present. Also, there is a divergence of V_{th} for PW1 in the vicinity of the ER. These observations make it impossible (as it will also be discussed later in the next section) to make any claim about the nature of driving mechanisms with full certainty.

The observation that the two prewavy instabilities have extremely similar appearances and properties, but might be caused by different mechanisms, is striking. Both regions form patterns on the order of hours, or days, versus the minutes it takes for the parallel stripes at low frequencies or for standard Carr-Helfrich patterns in other materials. Both patterns are only visible under crossed polarizers, indicating that director distortion remains in the xy-plane. Both have stripes that are perpendicular to the initial director orientation and have $\lambda \sim 3d-4d$. Both patterns develop disclinations, which evolve into "wavy" patterns [43] at voltages much greater than the threshold. (Which were also viewed through crossed polarizers, see Fig. 10.) All these optical properties are those of the previously described prewavy pattern.

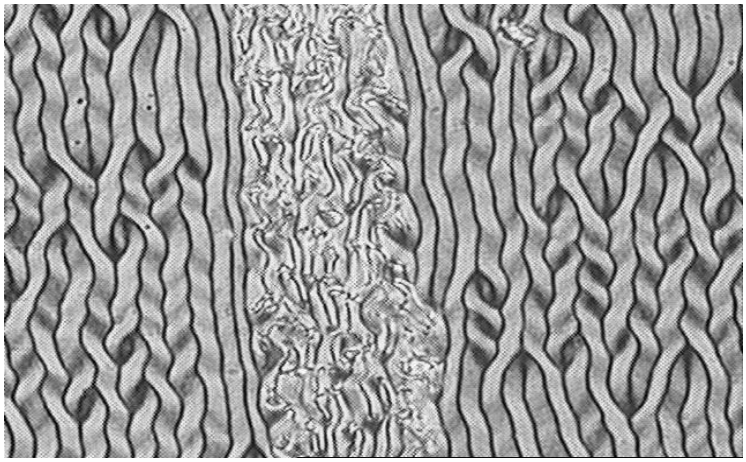

Figure 10: Example of the wavy pattern, which is seen in the center region of the image.

The wavelength was measured at different points in the frequency-voltage plane in four different ways. The points could be reached quasi-statically by holding one parameter fixed and varying the other slowly (with $dV/dt \sim 0.001$V/s or $df/dt \sim 1$Hz/s), rates of change increased to faster than about 0.005V/s or 10Hz/s would produce different patterns compared to the case when the parameters where changed more slowly. The pattern was allowed to relax for one hour after the point was reached. A video camera and a frame grabber were then used to capture an image of the pattern. The camera was oriented so that the stripes were vertical in the captured image (as in Fig. 5c). Then one color channel of the recorded RGB image was selected. The color values (0-255) from each pixel in a vertical column were summed and divided by the number of pixels in the column to get the average instensity. This was repeated for every column in the image. This procedure provides an averaged intensity profile across the stripes. Next, the FFT of this profile was taken. The wavelength and its uncertainty could be obtained from the locations of the first 4 or 5 FFT peaks (for a complete description of this method see [44]). The choice of color channel used to calculate the averaged intensity profile had no effect on the results.

Slowly varying the voltage with f fixed or slowly varying the frequency with V fixed, to reach the same point in the $V-f$ space, produced patterns with wavelengths that agreed with each other. In contrast, a different route to reach the same point in the $V-f$ space was a rapid change of one of the parameters (going from an intial value to a final value in about 1s), while the other was held fixed. Again, after one hour the wavelength was measured as above. Quickly changing the voltage at constant f, or the frequency at constant V, again produced the same wavelengths. However, the final wavelength observed (described below) differed substantially from that obtained using the previously described, quasi-static route.

Figure 13 shows that PW1 and PW2 exhibit similiar qualitative behavior in regards to how the wavelength varies with ε and f, where $\varepsilon = \frac{V^2-V_{th}^2}{V_{th}^2}$. Quickly varying one parameter produced a pattern that contained many more dislocations, of both the types shown in Fig. 11, than a pattern produced by slowly varying a parameter. Quick variations produced a pattern with a shorter wavelength than did slow variations. Also, after a period of 48 hours it was found that PW1 and PW2 patterns with dislocations, created by quickly varying the voltage, would relax to dislocation free patterns with a slightly longer wavelength (than what was found after one hour). Likewise, patterns formed by slowly varying the voltage would relax to a dislocation free pattern with a slightly shorter wavelength (than what was found after one hour), i.e. the wavelengths

http://www.e-lc.org/docs/2005_04_15_13_57_18

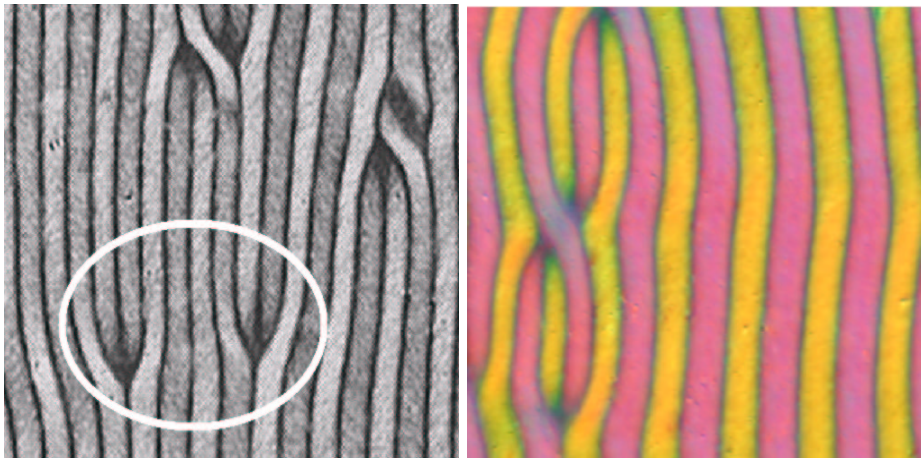

Figure 11: Examples of the two main types of dislocations which form in the prewavy regions. (a) The stripes split apart. (b) A close up of the stripes appearing to cross over, or twist around each other.

of the quickly varied and slowly varied patterns converge to an intermediate value after a certain time. This supports the idea that one stable, history independent, pattern would be seen given enough time.

Another interesting pattern, which we will call the "knitting" instability (Fig. 12), was produced by abruptly raising the voltage from one of the prewavy states. After several hours the knitting instabilitity would relax to a stripe pattern with dislocations, and would proceed to behave as the quickly varied state mentioned above. Several different types of long wavelength instabilities have been observed in other materials during system relaxation from an initial state to a final state after a change of a control parameter; e.g. the Eckhaus, the zigzag, and the skewed varicose instabilities [45]. The knitting instability is believed to represent a new long wavelength relaxation mechanism, which has not been previously observed.

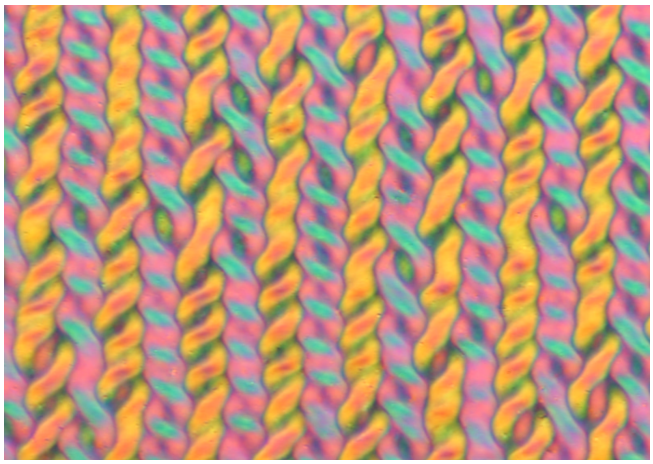

Figure 12: The "knitting" instability. It is produced by abruptly raising the voltage from one of the prewavy states.

All measurements from the previous sections were made with crossed polarizers. This configuration provides the best contrast for both PW1 and PW2. These patterns are also visible under nearly parallel polarizers with reduced contrast, but with one polarizer removed the pattern can not be optically discerned. The darker stripes in the prewavy patterns are produced by regions in which the director is roughly parallel, or perpendicular, to the polarizer. In this configuration the analyzer will block out the light. The brighter stripes are produced by regions where the director is at an angle to the polarizer. When the sample is rotated between crossed polarizers by 90° the directions parallel and perpendicular to the polarizer interchange but the intensities remain unchanged by this operation, thus the optical appearance of the pattern has a 90°

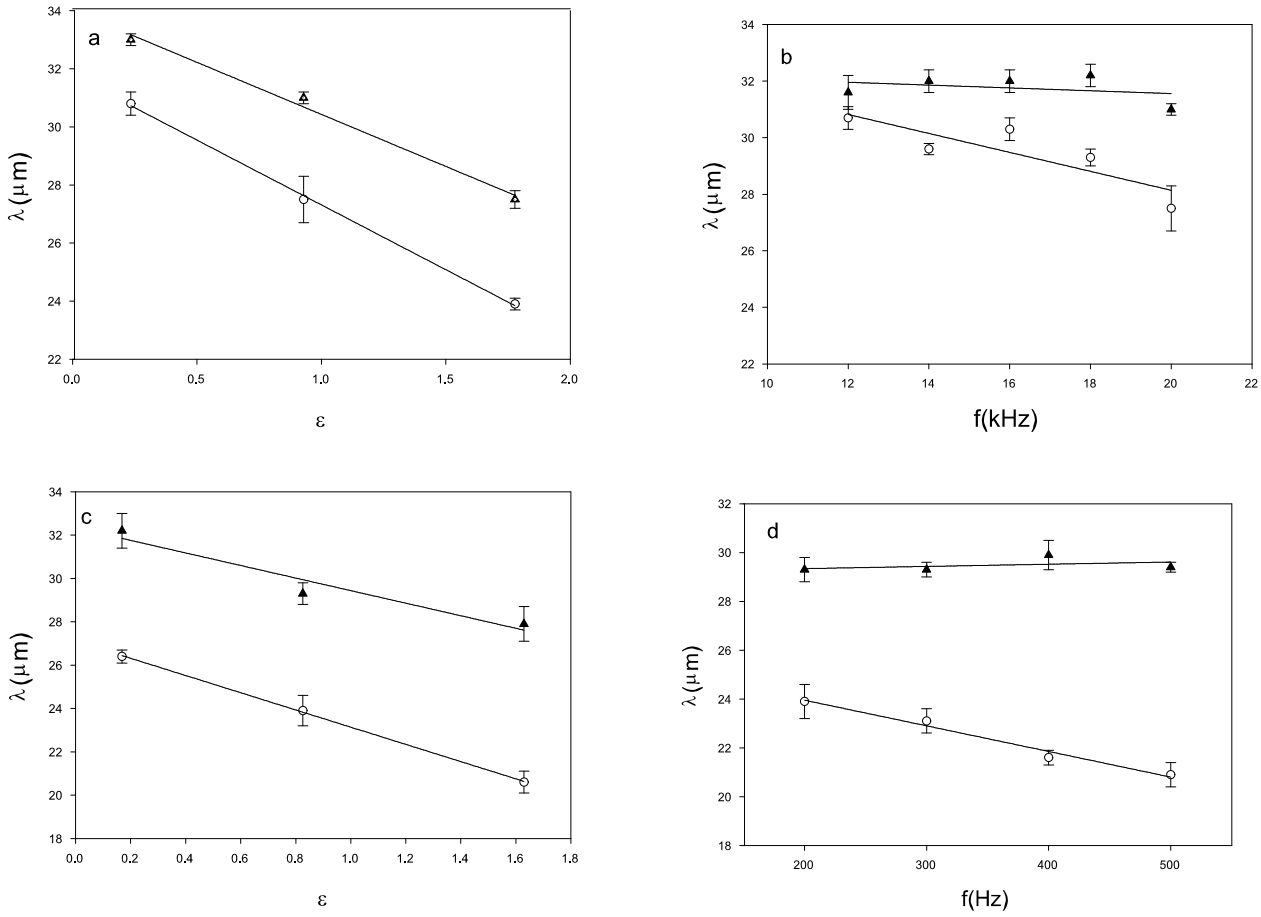

Figure 13: (a)Wavelength as a function of ε at 20kHz for PW1. (b)Wavelength as a function of frequency at 25V_{rms} for PW1. (c) Wavelength as a function of ε at 200Hz for PW2. (d) Wavelength as a function of frequency at 25V_{rms} for PW2. In all charts the solid triangles and the open circles represent the pattern achieved by slowly varying and by quickly varying the voltage, respectively. All measurements were made on a 10μm sample at 70°C.

periodicity with respect to sample rotation. If the sample is rotated 45°, with respect to its initial position, the director for the darker stripes will be at an angle of 45° to the polarizer, which produces the greatest possible passage of light. As a result the darkest regions become the brightest, which means that the pattern is inverted from its initial state.

These observations reveal that the prewavy stripes are due to periodic director modulations in the xy-plane [12, 17]. The voltage and frequency dependence of these director modulations were measured by rotating[10] [11] ¡phifit.eps¿ ¡i the sample under crossed polarizers. Initially, the sample was positioned so that the x-axis was aligned with a polarizer. Then the sample was rotated in one direction until the optical intensity was minimized for the stripes that were initially bright, i.e. until the director of those stripes was aligned with the polarizer. This was then repeated with the sample being rotated in the opposite direction. The images obtained by rotations in opposite directions were inverted, which indicates that the director modulation is symmetric with respect to the initial director orientation ($\hat{x}$).

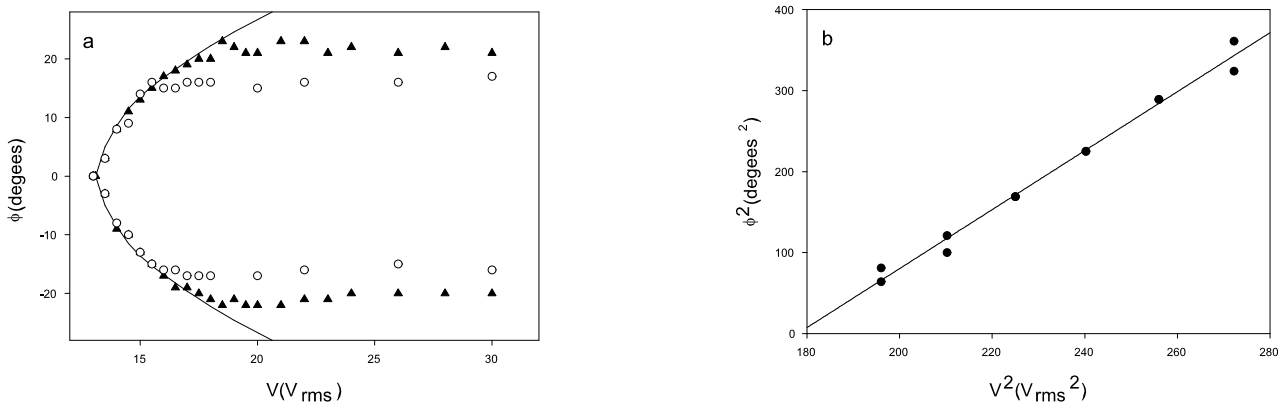

Figure 14: (a) Maxima of the azimuthal director modulation measured at 20kHz and 70°C. The solid triangles and the open circles show the director angle found by slowly varying and by quickly varying the voltage, respectively. The solid line shows the fit to Eq. (1) with $\phi_0 = 22.4°$ for the case where the voltage was slowly varied. (b) The goodness of the fit can be better demonstrated by manipulating Eq. (1) to the form $\phi^2 = (\phi_0/V_{th})^2 V^2 - {\phi_0}^2$, which more clearly shows the linear relation between ϕ^2 and V^2. Again, this was done for the case where the voltage was slowly varied. The fact that the ϕ values saturated at higher voltages made it difficult to discern the point where the quadratic behavior ended, so there is an amount of uncertainty introduced into the fit of the straight line depending on how many data points are used.

The voltage dependence was measured at 100Hz and 20kHz by slowly varying the voltage and then recording the angle, ϕ, the director in the initially bright stripes made with respect to the x-axis. This was then repeated with the voltage being quickly varied. (In both instances the voltage was changed in a manner similar to that described in the previous sections.) Similar measurements were made when varying the frequency at a fixed voltage. The amplitude of director modulations showed no frequency dependence in the observed region in either case.

Below the threshold voltage $\phi(V) = 0$. For $V > V_{th}$, ϕ exhibits a supercritical pitchfork bifurcation. Figure 14a shows that $\phi(V)$ saturates at a value of about 23° for the slowly varied pattern and about 18° for the quickly varied pattern, in both cases saturation occurs at voltages well above V_{th}. At 100Hz (PW2), the director has a behavior similar to that of the 20kHz (PW1) case (regarding the shape and the saturation values of the $\phi(V)$ curve), though over a different voltage range (40 – 50V). Figure 14 also shows that the amplitude of the azimuthal director modulation obtained by slowly varying a parameter can be well fit by the formula

$$\phi(\varepsilon) = \phi_0 \sqrt{\frac{V^2 - V_{th}^2}{V_{th}^2}} \tag{1}$$

for voltages slightly above V_{th} [17].

The value of $\phi(\varepsilon)$ seems to be dependent on the way in which the point in the $V-f$ space was reached, similar to the dependence shown for the wavelength. Also, the angular modulations of the states reached by quickly and slowly varying the voltage tend to converge to an intermediate value over time. This seems to show that a coupling between λ and ϕ can produce two quasi-stable history dependent states, which exist for at least 24 hours until the wavelengths and director modulations of the two states converge to form one stable state with intermediate λ and ϕ values.

The PW regimes had wider stripes and larger scale patterns than the PS region, this made it possible to observe flow via dust particles. The flow was very slow, taking up to several hours to move across the field of view (about 500μm) in some cases. Pictures were taken in five minute intervals and then viewed to track the motion of the dust particles. The "zig-zag" flow along the director (described in Ref. [18]) was the most frequently observed scenario. Dust particles were also observed to move in opposite directions, parallel to the stripes. The extremely low velocity of the flow prevented us from making quantitative measurements of the flow patterns.

IV. Conclusion

In summary, we have observed and described three instabilities, along with a region void of EC, in the bent core nematic ClPbis10BB. The PS instability, observed at low frequencies, consists of a pattern of narrow stripes that run roughly parallel to the initial director orientation and have a linear threshold curve. The PW1 instability appears to represent an excellent example of the previously described prewavy instability, which is characterized by a wide stripe pattern and director modulation in the xy-plane. The PW2 instability has nearly identical optical and dynamic properties to those of PW1, but the two instabilities show qualitatively different threshold behavior. The PW1 and PW2 regions are separated by the ER, where no EC was observed at fields higher than 12V/μm. These observations leave many questions unanswered, as the formation mechanisms for these regions are not yet understood.

In the previous section it was suggested that the PS is driven by an isotropic mechanism. However, there is also the possibility that the PS is caused by the flexoelectric effect. Banana shaped liquid crystals are expected to exhibit strong flexoelectric effects because of their shape [4], and the flexoelectric effect has been reported to produce two kinds of patterns composed of parallel stripes with the wavelength on the order of d; one at low frequencies [9, 10, 46–49] and another at high frequencies [9].

Patterns produced by the low frequency flexoelectric effect are best viewed with light polarized parallel to the x-axis (near onset) [46]. They possess λ varying as $1/V$, a threshold voltage that shows little change with respect to temperature or cell thickness, and they exhibit a frequency dependence similar to that of the conduction regime in a Carr-Helfrich type instability [9, 49]. PS does not show any of these characteristics. Instead, in PS, λ was seen to maintain a nearly constant value while the applied voltage is changed. $V_{th}(f)$ shows a linear frequency dependence (Fig. 6). $V_{th}(f)$ varies with changes in d, or temperature. And finally, as mentioned above, PS is best viewed through nearly crossed polarizers. Because of these considerations, we conclude that PS is not caused by the low frequency flexoelectric effect.

The high frequency longitudinal rolls observed by Blinov, et al [9] were not related to flexoelectricity at the time of their discovery. It was proposed later in Ref. [49] that the reported pattern might be caused by the flexoelectric effect. This high frequency flexoelectric pattern consists of randomly oriented linear domains, and was observed in a calamitic $(--)$ material. These domains had periods less than d, which were independent of temperature. V_{th} for these patterns showed a linear frequency dependence and was proportional to the cell thickness, i.e. had a field threshold. PS shares many of these traits. PS was oriented in small domains that went from parallel to oblique with λ slightly less than d. PS showed a weak temperature dependence and V_{th} for PS exhibited a linear frequency dependence. V_{th} for PS also appeared to vary with cell thickness.

It was proposed in Ref. [49] that the high frequency flexoelectric regime in $(--)$ materials is analogous to the dielectric regime in $(-+)$ materials, i.e. it is an anisotropic mode. It was stated in the previous section while discussing PS that a divergence of V_{th} is generally expected near the clearing point for anisotropic mechanisms. However, this is not always the case. Certain materials that exhibit Carr-Helfrich type instabilities, such as Phase 5 (Merck), do not show a divergence in V_{th} at the clearing point. This apparent discrepancy is believed to be related to the nature of the N-I transition. A divergence is in fact only expected for weakly first order transitions, where the anisotropies go to zero almost continuously. If the anisotropies show only a weak temperature dependence then fall to zero suddenly at T_{NI}, a divergence might not be

http://www.e-lc.org/docs/2005_04_15_13_57_18

present. The substance ClPbis10BB exhibits a fairly large jump of ϵ_a near T_{NI} at 1kHz. Thus a lack of divergence of V_{th} near T_{NI} would not be surprising. It means that one cannot exclude the possibility that PS is driven by an anisotropic mechanism, like the high frequency flexoelectric mode mentioned above. If this were the case, PS might still be explained by the standard model after incorporating the flexoelectric effect.

Let us now focus on the prewavy modes PW1 and PW2. It was shown in the previous section that the characteristics of the PW1 instability correspond to those of the prewavy pattern [18], except for the frequency dependence of the thresholds. The optical appearance and the dynamical behavior of PW2 was found to be almost identical to those of PW1. Nevertheless, based on the differences in the temperature and frequency dependencies of the threshold voltages we suggested that PW1 and PW2 may be of different origins. PW2, possessing a divergent V_{th} at a sign inversion of σ_a, is very likely caused by an anisotropic mechanism. On the contrary, PW1, which seems to be unaffected by another sign inversion of σ_a, may be due to an isotropic mechanism. In the ER, which separates the two prewavy modes in frequency, the BCN studied is $(-+)$ so a Carr-Helfrich type instability could be expected, yet is not observed. There is no explanation as to why no EC exists in this region.

We should note, however, that one cannot exclude an alternative interpretation of the experimental findings. Based on their optical similarities, the idea that PW1 and PW2 are both formed by the same (supposedly isotropic) prewavy mechanism should also be considered. We have already argued above, that the temperature dependence of the thresholds near the clearing point does not allow a clear separation of anisotropic and isotropic pattern forming mechanisms, except in the presence of a pronounced divergence (which we do not have for PW2). It was stated earlier that the $V_{th}(f)$ curves and their temperature shift are different for PW1 and PW2 (see Fig. 8). It should be taken into account, however, that PW1 and PW2 occur in very different frequency ranges. If the relative changes are compared, i.e. by means of a logarithmic scale for f instead of a linear one, as in Fig. 4, the frequency dependence of V_{th} and its temperature shift become quite similar for PW1 and PW2. The divergence of threshold, and thus the opposite slope of V_{th} for PW1 and PW2, as well as the existence of ER in between them, then suggest that there is another process inhibiting the prewavy mechanism for some reason, and also preventing the occurrence of the Carr-Helfrich instability in the ER. We have already mentioned that the studied BCN exhibits a broad dielectric relaxation in the frequency range in question, which is responsible for the double sign change of σ_a shown in Fig. 3. This relaxation phenomenon might be the process interacting with the pattern formation process and suppressing electroconvection. (The inhibiting might be the strongest near the maximum of the dielectric loss, which occurs at the maximum of $|\sigma_a|$ near the center of the ER.) With these considerations, if there was no relaxation present, one should see just a single type of prewavy pattern, without ER, in the whole frequency range.

Unfortunately no rigorous theoretical treatment of the isotropic electroconvection modes has been developed at this time which could give an account of the mechanism of the prewavy pattern. Nor has the influence of a frequency dependent ϵ_a and σ_a been fully analyzed within the framework of the standard model, which could answer the speculations above. The few reports of electroconvection associated with dielectric relaxation [38, 50] concern substances applicable for dual frequency addressing , i.e. exhibiting a sign inversion of ϵ_a at increasing f, but having $\sigma_a > 0$ at all frequencies, which are not relevant to our case.

Acknowledgements

We have benefited from fruitful discussions with A. Buka and technical assistance from G. Liao. This work was supported by the NSF (DMR-9988164 and OISE-0225963) and the US Department of Education as well as the NSF-MTA-OTKA joint project #78 and the Hungarian Research Funds OTKA-T037336, OTKA-T032667, and NKFP-128/6.

References

[1] E. F. Carr. *Mol. Cryst. Liq. Cryst.*, 7:253, 1969.

[2] W. Helfrich. *J. Chem. Phys.*, 51:4062, 1969.

[3] L. M. Blinov and V. G. Chigrinov. *Electrooptic Effects in Liquid Crystal Materials.* Springer-Verlag, 1994.

[4] P. G. de Gennes and J. Prost. *The Physics of Liquid Crystals*. Oxford Science Publications, 1993.

[5] A. Buka and L. Kramer. *Pattern Formation in Liquid Crystals*. Springer-Verlag, 1996.

[6] A. Buka, B. Dressel, W. Otowski, K. Camara, T. Toth-Katona, L. Kramer, J. Lindau, G. Pelzl, and W. Pesch. *Phys. Rev. E*, 66:051713, 2002.

[7] B. Dressel and W. Pesch. *Phys. Rev. E*, 67:031707, 2003.

[8] E. Kochowska, S. Nemeth, G. Pelzl, and A. Buka. *Phys. Rev. E*, 70:011711, 2004. El. Liq. Cryst. Commun., <http://www.e-lc.org/docs/2004_01_23_11_12_27>.

[9] L. M. Blinov, M. I. Barnik, V. T. Lazareva, and A. N. Trufanov. *J. Phys. (Paris), Colloq.*, C3:C3–263, 1979.

[10] M. Goscianski and L. Leger. *J. Phys. (Paris), Colloq.*, C1:C1–231, 1975.

[11] P. Petrescu and M. Giurgea. *Phys. Lett. A*, 59:41, 1976.

[12] L. Nasta, A. Lupu, and M. Giurgea. *Mol. Cryst. Liq. Cryst.*, 71:65, 1981.

[13] A. N. Trufanov, M. I. Barnik, and L. M. Blinov. *JETP*, 51:314, 1980.

[14] S. Kai and K. Hirakawa. *Solid State Commun.*, 18:1573, 1976.

[15] R. Ribotta and G. Durand. *J. Phys. (Paris), Colloq.*, 40:C3–334, 1979.

[16] W. Weissflog, G. Pelzl, H. Kresse, and D. Demus. *Cryst. Res. Technol.*, 23:1259, 1988.

[17] J.-H. Huh, Y. Yusuf, Y. Hidaka, N. Eber, T. Toth-Katona, A. Buka, and S. Kai. *Mol. Cryst. Liq. Cryst.*, 364:111, 2001.

[18] J.-H. Huh, Y. Yusuf, Y. Hidaka, and S. Kai. *Phys. Rev. E*, 66:1063, 2002.

[19] S. Komineas, H. Zhao, and L. Kramer. *Phys. Rev. E*, 67:031701, 2003.

[20] M. I. Barnik, L. M. Blinov, S. A. Pikin, and A. N. Trufanov. *JETP*, 45:396, 1977.

[21] S. A. Pikin and V. G. Chigrinov. *JETP*, 51:123, 1980.

[22] T. Niori, T. Sekine, J. Watanabe, T. Furukawa, and H. Takezoe. *J. Mater. Chem.*, 6(7):1231, 1996.

[23] T. Sekine, T. Niori, M. Sone, J. Watanabe, S. W. Choi, Y. Takanishi, and H. Takezoe. *Jpn. J. Appl. Phys.*, 36:6455, 1997.

[24] D. R. Link, G. Natale, R. Shao, J. E. Maclennan, N. A. Clark, E. Korblova, and D. M. Walba. *Science*, 278:1924, 1997.

[25] J. A. Oliveras, S. Stojadinovic, T. J. Dingemans, S. Sprunt, and A. Jakli. *Phys. Rev. E*, 68:041704–1–6, 2003.

[26] B. R. Acharya, A. Primak, T. J. Dingemans, E. T. Samulski, and S. Kumar. *Pramana*, 61:231, 2003.

[27] L. A. Madsen, T. J. Dingemans, M. Nakata, and E. T. Samulski. *Phys. Rev. Lett.*, 92(14):145505, 2004.

[28] B. R. Acharya, A. Primak, and S. Kumar. *Phys. Rev. Lett.*, 92(14):145506, 2004.

[29] T. C. Lubensky and L. Radzihovsky. *Phys. Rev. E*, 66:031704–1–27, 2002.

[30] J. Matraszek, J. Mieczkowski, J. Szydlowska, and E. Gorecka. *Liq. Cryst.*, 27:429, 2000.

[31] I. Wirth, S. Diele, A. Eremin, G. Pelzl, S. Grande, L. Kovalenko, N. Pancenko, and W. Weissflog. *J. Mater. Chem.*, 11:1642, 2001.

[32] W. Weissflog, H. Nadasi, U. Dunemann, G. Pelzl, S. Diele, A. Eremin, and H. Kresse. *J. Mater. Chem.*, 11:2748, 2001.

[33] E. Matyus and K. Keseru. *J. Mol. Struct.*, 543:89, 2001.

[34] T. J. Dingemans and E. T. Samulski. *Liq. Cryst.*, 27:131, 2000.

[35] K. Fodor-Csorba, A. Vajda, G. Galli, A. Jakli, D. Demus, S. Holly, and E. Gacs-Baitz. *Macromol. Chem. Phys.*, 203:1556, 2002.

[36] E.H.C. Co, Tokyo, Japan.

[37] Hp. Schad, B. Scheuble, and J. Nehring. *J. Chem. Phys.*, 71:5140, 1979.

[38] W. H. De Jeu, C. J. Gerritsma, and W. J. A. Goosens. *Phys. Lett.*, 39A:355, 1972.

[39] F. Brochard. *Mol. Cryst. Liq. Cryst.*, 23:51, 1973.

[40] H. Kneppe, F. Schneider, and N. K. Sharma. *J. Chem. Phys.*, 77:3203, 1982.

[41] K. Skarp, S. T. Lagerwall, and B. Stebler. *Mol. Cryst. Liq. Cryst.*, 60:215, 1980.

[42] M. Cui and J. R. Kelly. *Mol. Cryst. Liq. Cryst.*, 331:1909, 1999.

[43] J.-H. Huh, Y. Hidaka, A. Rossberg, and S. Kai. *Phys. Rev. E*, 61:2769, 2000.

[44] J. T. Gleeson. *Phys. Rev. E*, 54:6424, 1996.

[45] S. Kai, Y. Adachi, and S. Nasuno. *Spatio-Temporal Patterns.* edited by P. Cladis and Palffy-Muhoray. Addison-Wesley Publishing Company, 1995.

[46] M. I. Barnik, L. M. Blinov, B. A. Umansky, and A. N. Trufanov. *J. Phys. (Paris)*, 39:417, 1978.

[47] L. M. Blinov. *J. Phys. (Paris), Colloq.*, 40:C3–247, 1979.

[48] Y. Bobylev, V. G. Chigrinov, and S. Pikin. *J. Phys. (Paris), Colloq.*, 40:C3–331, 1979.

[49] N. V. Madhusudana and V. A. Raghunathan. *Liquid Crystals*, 5:1789, 1989.

[50] V. G. Chigrinov, A. Sparavigna, and A. Strigazzi. *Phys. Rev. E*, 53:4918, 1996.